

# Bis-(*N*-ethylphenyldithiocarbamato)palladium(II) as molecular precursor for palladium sulfide nanoparticles

Athandwe M. Paca, Peter A. Ajibade\*

School of Chemistry and Physics, University of KwaZulu-Natal, Private Bag X01, Scottsville, Pietermaritzburg 3200, South Africa



## ARTICLE INFO

### Article history:

Received 5 March 2021

Revised 12 May 2021

Accepted 22 May 2021

Available online 28 May 2021

### Keywords:

Metal sulfide

Thermal decomposition

Octadecylamine

Single-source molecule

Palladium(II) dithiocarbamate

## ABSTRACT

Bis(*N*-ethylphenyldithiocarbamato)palladium(II) was synthesized and characterized by elemental analysis, spectroscopic techniques and single crystal X-ray crystallography. The molecular structure confirmed the *N*-ethylphenyldithiocarbamato anions coordinated bidentately to the Pd(II) ion through the sulfur atoms and resulted in the formation of a square planar geometry. The complex was used as a single-molecule precursor and thermolyzed at three different temperature to investigate the influence of the thermolysis temperature on the optical and morphological properties of the as-prepared palladium sulfide nanoparticles. The pXRD proved that variation of the thermolysis temperature resulted in palladium sulfide nanoparticles with different diffraction patterns. TEM images showed that nanoparticles with particle sizes of 2.01–2.50 nm, 4.00–4.86 nm and 2.53–4.12 nm were obtained at 160, 200 and 240 °C, respectively. This revealed that increase in temperature resulted in larger nanoparticles but as temperature gets higher the particle size distribution becomes non-uniform. SEM micrographs revealed that the nanoparticles have a rough surface with different surface morphologies. The optical band gap ( $E_g$ ) range between 4.90–5.02 eV and was slightly increased when the temperature was increased.

© 2021 Elsevier B.V. All rights reserved.

## 1. Introduction

Metal sulfide are important class of compounds that are being studied due to the existence of different crystalline structures [1]. They are major group of minerals with various structural phases with general formula  $M_xS_y$  [2,3]. They have unique electrical, magnetic and optical properties that make them useful in solar cells [4], fuel cells [5], gas sensors [1] and laser devices [6]. Different fabrication methods have been used to synthesized metal sulfide nanoparticles [7], these include chemical vapour deposition [8,9], hydrothermal [10,11], solvothermal [12,13] and thermal decomposition of single source precursors [14–16]. Thermal decomposition of single-source precursors (SSP) method has been explored for the fabrication of metal sulfide nanoparticles especially from metal dithiocarbamate complexes in appropriate capping agents [17].

The formation of nanoparticles through the thermal decomposition method is influenced by the reaction conditions such as the temperature, capping agents, thermolysis time, and the single source precursor complexes. Research have shown that thermolysis temperature influences the physical attributes of nanoparticles such as shape, size, particle size distribution and crystallinity [18,19]. Capping agents acts as protective surface atoms on the

nanoparticles to prevent aggregation, protects the particles from its surroundings and affords electronic equilibrium to the surface of the nanoparticles [20–24]. The capping agent bonds covalently to surface metal atoms like a Lewis base and passivate the nanoparticles [25,26]. Metal dithiocarbamate complexes are well-known single-source precursors for the preparation of metal sulfide nanoparticle due to their facile synthesis and the ability to modify their volatility and decomposition attributes based on the amine substituents [27]. This synthetic method eliminates impurities as the metal is already coordinated to the sulfide atoms.

Palladium sulfide exist in various crystalline phases. Ehsan et al. [28] prepared vysotskite structured PdS thin film with a direct band gap of 1.56 eV from a palladium(II) dithiocarbamate complex. Ajibade and Nqombolo [29] thermolyzed palladium(II) imidazolyl dithiocarbamate complex in hexadecylamine at 220 °C to obtained PdS nanoparticles. The nanoparticles showed crystalline sizes ranging between 10.65 and 16.25 nm with an optical band gap of 3.90 eV. The particle size of the nanoparticles is influenced by the reaction parameters such as the duration of the reaction, thermolysis temperature and nature of the precursor [25]. Variation of these reaction conditions influences the crystalline phase and particle size of the nanoparticles. In this work, bis(*N*-ethylphenyldithiocarbamato)palladium(II) was synthesized and characterized by elemental analysis, spectroscopic techniques and single crystal X-ray crystallography. The compound was

\* Corresponding author.

E-mail address: [ajibadep@ukzn.ac.za](mailto:ajibadep@ukzn.ac.za) (P.A. Ajibade).

thermolyzed at three different temperatures to prepare palladium sulfide nanoparticles and investigate the effect of decomposition temperature on the optical and morphological properties of the as-prepared PdS nanoparticles.

## 2. Experimental

### 2.1. Reagents and solvents

All chemicals and solvents were of analytical grades purchased from Merck chemical and were used as obtained without further purification. Chemicals and solvents used: *N*-ethylaniline, aqueous ammonia, carbon disulphide, diethyl ether, palladium nitrate dihydrate ( $\text{Pd}(\text{NO}_3)_2 \cdot 2\text{H}_2\text{O}$ ), chloroform, dimethyl sulfoxide (DMSO), trioctylphosphine (TOP), octadecylamine (ODA) and methanol. The  $^1\text{H}$  and  $^{13}\text{C}$  NMR spectra were recorded on Bruker Biospin 600 MHz spectrometer. Samples were prepared in deuterated water ( $\text{D}_2\text{O}$ ) and deuterated chloroform ( $\text{CDCl}_3$ ). Residual signals of  $\text{D}_2\text{O}$  ( $\delta = 4.79$  ppm for  $^1\text{H}$  NMR) and  $\text{CDCl}_3$  ( $\delta = 7.26$  ppm for  $^1\text{H}$  NMR and  $\delta = 77.16$  ppm for  $^{13}\text{C}$  NMR) were used as the internal reference. Chemical shifts were reported in parts per million (ppm). The spectra were processed using Bruker TopSpin 4.0.3 NMR prediction software. The FTIR spectra were recorded by an Agilent Technologies Cary 630 FTIR spectrometer (4000 – 650  $\text{cm}^{-1}$ ). Electronic spectra measured by a Perkin Elmer Lambda 25 spectrometer from 200 to 700 nm at room temperature. Powder X-ray diffraction (pXRD) patterns were recorded by a Bruker D8 advanced diffractometer using  $\text{Cu K}\alpha$  radiation. Samples were mounted on a flat steel and scanned from 5 to 70°. Transmission electron microscopy (TEM) images were obtained from JEOL –1400 electron microscope while high resolution transmission electron microscopy (HRTEM) images were obtained from JEOL HRTEM-2100. The nanoparticles were dispersed in distilled water and dropped on carbon coated copper grid and evaporated at room temperature. Scanning electron microscopy (SEM) images were obtained by a ZEISS EVO LS 15 electron microscope. Electron dispersive X-ray spectroscopy (EDX) spectra were obtained by ZEISS EVO LS 15 electron microscope. The nanoparticles were fixed on aluminium studs by a double-sided carbon tape and coated with gold. The ligand ammonium *N*-ethylphenyldithiocarbamate was prepared as reported previously [30]

### 2.2. Synthesis of bis(*N*-ethylphenyldithiocarbamato)palladium(II)

The Pd(II) precursor complex was prepared as presented in Scheme 1. In a typical synthesis, ammonium *N*-ethylphenyldithiocarbamate ligand (0.40 g, 1.88 mmol) dissolved in distilled water (50 mL) was added to an aqueous solution of  $\text{Pd}(\text{NO}_3)_2 \cdot 2\text{H}_2\text{O}$  (0.25 g, 0.94 mmol) with constant stirring. A dusty orange precipitate formed immediately, and the reaction was continued for 2 h. After which chloroform was added, two phases (aqueous and organic) formed. The two phases were separated using a separating funnel. The aqueous phase was further extracted with chloroform. The extracts were combined with the organic phase and left to dry in open air. Yield: 27.05 %. Selected FTIR,  $\nu(\text{cm}^{-1})$ : N-C (1469), C-S (1276), C=S (989).  $^1\text{H}$  NMR ( $\text{CDCl}_3$ , ppm): 7.44–7.48 (t, 2H), 7.40–7.242 (t, 1H), 7.21–7.24 (d, 2H), 4.04–4.12 (d, 2H), 1.23–1.28 (t, 3H).  $^{13}\text{C}$  NMR ( $\text{D}_2\text{O}$ , ppm): 127.63–139.95 ( $\text{C}_6\text{H}_5$ ), 48.06 ( $-\text{CH}_2-$ ), 12.68 ( $-\text{CH}_3$ ), 213.42 (C-S). Anal. Calc. for  $\text{C}_{18}\text{H}_{20}\text{N}_2\text{PdS}_2$ : C, 49.71; H, 4.63; N, 6.44. Found: C, 49.33; H, 4.24; N, 6.37.

### 2.3. X-ray data collection

A single crystal of bis(*N*-ethylphenyldithiocarbamato)palladium(II) was obtained by slow evaporation of the compound solution in

**Table 1**

Summary of crystal data and structure refinement for bis(*N*-ethylphenyldithiocarbamato)palladium(II).

Identification code	Compound
Empirical formula	$\text{C}_{18}\text{H}_{20}\text{N}_2\text{PdS}_2$
Formula weight (g/mol)	499
Temperature (K)	100(2)
Wavelength	1.54178
Crystal system	Monoclinic
Space group	$\text{P}2_{1/n}$
Unit cell dimensions (Å)	
$a$ (Å)	7.3467(4)
$\alpha$ (°)	90
$b$ (Å)	6.9378(3)
$\beta$ (°)	95.466(3)
$c$ (Å)	19.7917(8)
$\gamma$ (°)	90
Volume (Å <sup>3</sup> )	1004.19(8)
$Z$	4
Calculated density (Mg/m <sup>3</sup> )	1.650
Absorption coefficient (mm <sup>-1</sup> )	11.364
F(000)	505
Crystal size (mm <sup>3</sup> )	0.370 × 0.060 × 0.050
Theta range for data collection (°)	4.488 to 69.259
Limiting indices	$-8 <= h <= 8, -8 <= k <= 8, -23 <= l <= 23$
Reflections collected / unique	1781 / 1781 [R(int) = ?]
Completeness to theta = 25.242 (%)	96.8 %
Absorption correction	Semi-empirical from equivalents
Max. and min. transmission	0.7530 and 0.3783
Refinement method	Full-matrix least-squares on $F^2$
Data / restraints / parameters	1781 / 0 / 117
Goodness-of-fit on $F^2$	1.179
Final R indices [ $I > 2\sigma(I)$ ]	R1 = 0.0358, wR2 = 0.0833
R indices (all data)	R1 = 0.0392, wR2 = 0.0851
Largest diff. peak and hole (e.Å <sup>-3</sup> )	0.650 and -0.667

dimethyl sulfoxide (DMSO) at room temperature. A crystal with dimensions  $0.370 \times 0.060 \times 0.050$  mm<sup>3</sup> was isolated under oil and fixed on a MITIGEN crystal mounter. The data was gathered by a Bruker APEX-II CCD diffractometer fitted with an Oxford Cryosystems low temperature instrument, running at  $T = 100(2)$  K. The structure was resolved by the She1XS-2013 software and refined using She1XL 2016/6 version [31,32].

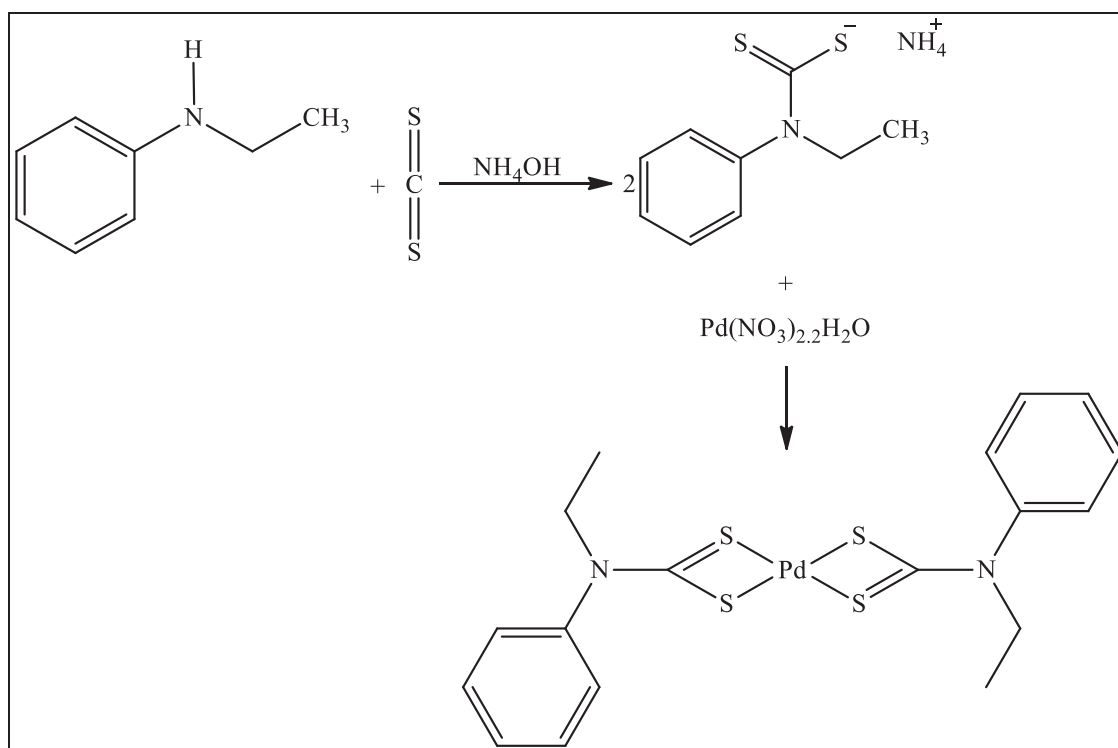
### 2.4. Synthesis of palladium sulfide nanoparticles

Bis(*N*-ethylphenyldithiocarbamato)palladium(II) (0.1 g) dispersed in trioctylphosphine (TOP) (2 mL) was injected into 2 g of octyldecylamine (ODA) stabilized at 160, 200 and 240 °C under nitrogen flow and the reaction was maintained for 1 h. After, the reaction was cooled down to about 65 °C and cold methanol was added. The nanoparticles were separated by centrifugation, washed several times with cold methanol and dried. The prepared nanoparticles were labelled PdS1, PdS2 and PdS3 for nanoparticles prepared at 160, 200 and 240 °C, respectively.

## 3. Results and discussion

### 3.1. Molecular structure of bis(*N*-ethylphenyldithiocarbamato)palladium(II)

Single crystals of bis(*N*-ethylphenyldithiocarbamato)palladium(II) suitable for X-ray crystallography were obtained by slow evaporation of DMSO solution of the compound. The molecular structure of the complex is presented in Fig. 1 and the unit cell packing diagram in Fig. S1. Crystallographic and refinement information are given in Table 1. Selected bond lengths and angles are provided in Table 2. The crystal structure of bis(*N*-ethylphenyldithiocarbamato)palladium(II) is made up of two *N*-ethylphenyldithiocarbamato anions bonded to a Pd(II) metal cen-



**Scheme 1.** Synthesis of *N*-ethylphenyldithiocarbamate ligand and bis(*N*-ethylphenyldithiocarbamato)palladium(II).

tre. The complex resides on a monoclinic  $P_{21/n}$  site with four molecules occupying the unit cell ( $Z = 4$ ). The Pd(II) ion is coordinated to four sulfur atoms from the two dithiocarbamate anions to form a square planar geometry similar to other related compounds in literature [33–36]. In the Pd(II) complex, Pd–S bond lengths of 2.3173 and 2.3350 Å and comparable to 55 related compounds found from the Cambridge Structural Database (CSD) records [37–39]. The S–Pd–S bond angle of 75.64(4)° show a slight devia-

tion in comparison to the previous reported related compounds with an average value of 75.28° for the cited complexes found in literature [36,40–42]. The C–S bond lengths of 1.725(5) and 1.719(5) Å are intermediate between double and single bond suggesting the resonance phenomenon in the  $\text{CS}_2$  moiety and comparable to 109 related structures retrieved from CSD database [43–46]. The N(1)–C(1) bond distance of 1.317(6) Å is very close to the mean value of 1.332 Å recorded for 53 related compounds in the

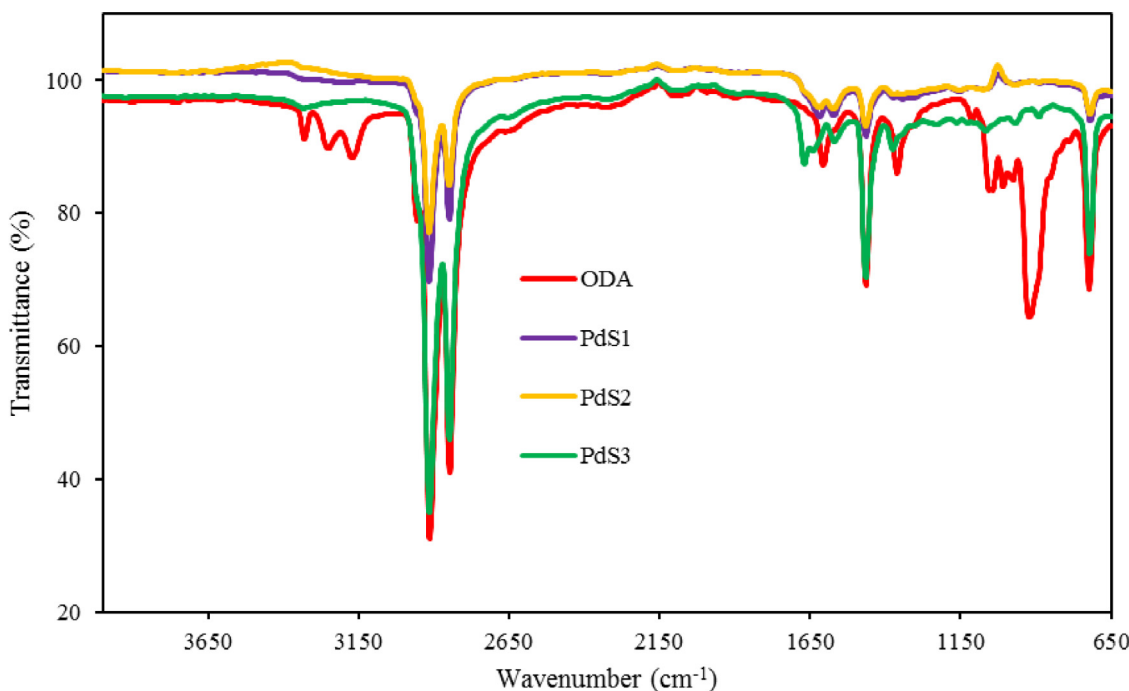


**Fig. 6.** FTIR spectra of ODA and the PdS nanoparticles prepared from different temperatures.

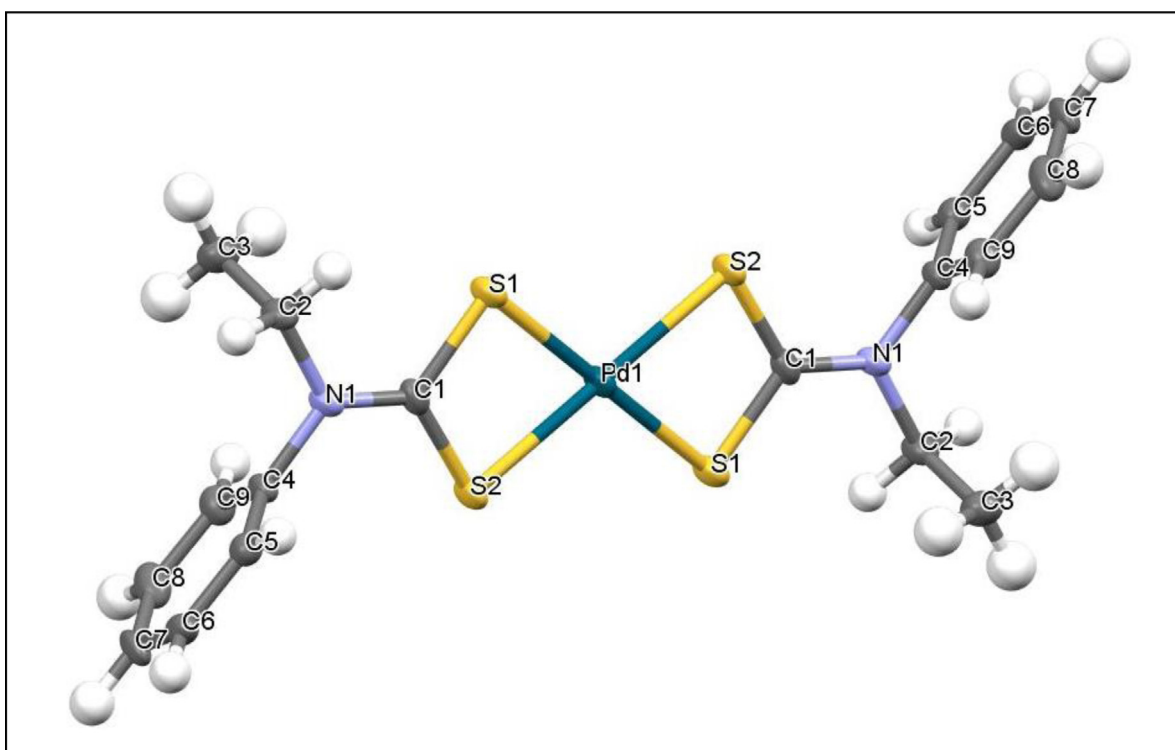


**Fig. 1.** Molecular structure of bis(*N*-ethylphenyldithiocarbamato)palladium(II) showing 50 % probability displacement ellipsoid and atom labelling. The hydrogen atoms are excluded for clearness.

**Table 2**  
Bond lengths (Å) and angles (°) for bis(*N*-ethylphenyldithiocarbamato)palladium(II).

Bond length (Å)	Bond angles (°)	
Pd(1) - S(1)#1	2.3173(12)	S(1)#1-Pd(1)-S(1) 180.0
Pd(1) - S(1)	2.3173(12)	S(1)#1-Pd(1)-S(2)#1 75.64(4)
Pd(1) - S(2)#1	2.3350(11)	S(1)-Pd(1)-S(2)#1 104.36(4)
Pd(1) - S(2)	2.3349(11)	S(1)#1-Pd(1)-S(2) 104.36(4)
S(1) - C(1)	1.725(5)	S(1)-Pd(1)-S(2) 75.64(4)
S(2) - C(1)	1.719(5)	S(2)#1-Pd(1)-S(2) 180.000
N(1) - C(1)	1.317(6)	C(1)-S(1)-Pd(1) 86.40(17)
N(1) - C(4)	1.443(6)	C(1)-S(2)-Pd(1) 85.96(15)
N(1) - C(2)	1.483(6)	N(1)-C(1)-S(1) 123.6(4)
		N(1)-C(1)-S(2) 124.5(4)
		S(1)-C(1)-S(2) 111.9(3)
		C(1)-N(1)-C(4) 121.7(4)
		C(1)-N(1)-C(2) 121.8(4)

CSD database [47,48]. This bond implies a partial double bond behaviour because of higher electron density anticipated upon coordination, and delocalization of electron density in the dithiocarbamate moiety, as confirmed by FTIR and  $^{13}\text{C}$  NMR spectra. The molecular structure of the compound is like the reported bis(*N*-butylphenyldithiocarbamato)palladium(II) [48].

### 3.2. Spectroscopic studies

Dithiocarbamate ligands can be distinguished by the presence of the  $\text{NCS}_2^-$  dithiocarbamate moiety. A strong absorption band in the region  $1450 - 1590 \text{ cm}^{-1}$ , is due to the  $\nu(\text{C}-\text{N})$  (thioureide) stretching vibrations of the  $\text{N}-\text{C}=\text{S}$  system, the stretching vibrations in the region  $1150 - 1280 \text{ cm}^{-1}$  is attributed to  $\nu(\text{C}-\text{S})$  and a single sharp vibrational band in the region  $950 - 1050 \text{ cm}^{-1}$ , is ascribed to the  $\nu(\text{C}=\text{S})$  stretching vibration which denotes the symmetrical bidentate coordination of the ligand through the sulfur atoms of the dithiocarbamate anions to the Pd(II) centre [40,49].

In the FTIR spectrum of *N*-ethylphenyldithiocarbamate ligand, the  $\nu(\text{N}-\text{C})$  stretching frequency was observed at  $1585 \text{ cm}^{-1}$ ,  $\nu(\text{C}-\text{S})$  at  $1234 \text{ cm}^{-1}$  and  $\nu(\text{C}=\text{S})$  at  $988 \text{ cm}^{-1}$ . In the complex the  $\nu(\text{C}-\text{N})$  band shifted to  $1588 \text{ cm}^{-1}$ . The  $\text{CS}_2$  groups also shifted to higher frequencies. The presence of a single sharp  $\nu(\text{C}-\text{S})$  band in the spectrum of the complex implies that the ethylphenyldithiocarbamate anions coordinated bidentately to the Pd(II) center [50].

The electronic spectrum of the ligand in water showed two broad absorption bands with high intensity. The first band at  $260 \text{ nm}$  associated with the  $\pi \rightarrow \pi^*$  transitions of the  $\text{N}-\text{C}=\text{S}$  of the dithiocarbamate moiety [51]. The second absorption band at  $280 \text{ nm}$  was ascribed to the  $\pi \rightarrow \pi^*$  transitions of the  $\text{S}-\text{C}=\text{S}$  moiety [52]. Another band with very low intensity was observed at about  $453 \text{ nm}$ , attributed to the  $\text{n} \rightarrow \pi^*$  transition located on the sulfur atom. The electronic absorption spectrum of bis(*N*-ethylphenyldithiocarbamato)palladium(II) complex showed one strong broad band with an absorption maximum of  $311 \text{ nm}$ . This band was associated with the metal-to-ligand charge transfer ( $\text{M} \rightarrow \text{LCT}$ ) transitions due to the coordination of the ligand to the Pd(II). Since Pd(II) ion is a  $d^8$  configuration and all the electrons are paired, therefore no  $d-d$  bands were visible.

The  $^1\text{H}$  NMR of *N*-ethylphenyldithiocarbamate ligand showed a doublet at  $7.27-7.29 \text{ ppm}$ , a triplet at  $7.42-7.43 \text{ ppm}$  and a triplet at  $7.44-7.45 \text{ ppm}$  of the phenyl ring. The quartet observed at  $4.41 - 4.36 \text{ ppm}$  was assigned to the hydrogen atoms of the ethyl group and triplet at  $1.28 - 1.24 \text{ ppm}$  assign to methyl group. The  $^{13}\text{C}$  NMR showed signals at  $126.89-140.64 \text{ ppm}$  attributed to the  $(\text{C}_6\text{H}_5)$  of the phenyl group. The  $-\text{CH}_2-$  carbon signal appeared at  $53.21 \text{ ppm}$  and  $-\text{CH}_3$  signal was observed at  $11.70 \text{ ppm}$ . The signal due to the  $\text{C}-\text{S}$  bond was observed at  $210.85 \text{ ppm}$ . Similar bonds were observed when the ligand was coordinated to the Pd(II) ion to form bis(*N*-ethylphenyldithiocarbamato)palladium(II), except that a shift to an upfield environment was observed for the protons of the complex and the carbons shifted to a downfield environment. The

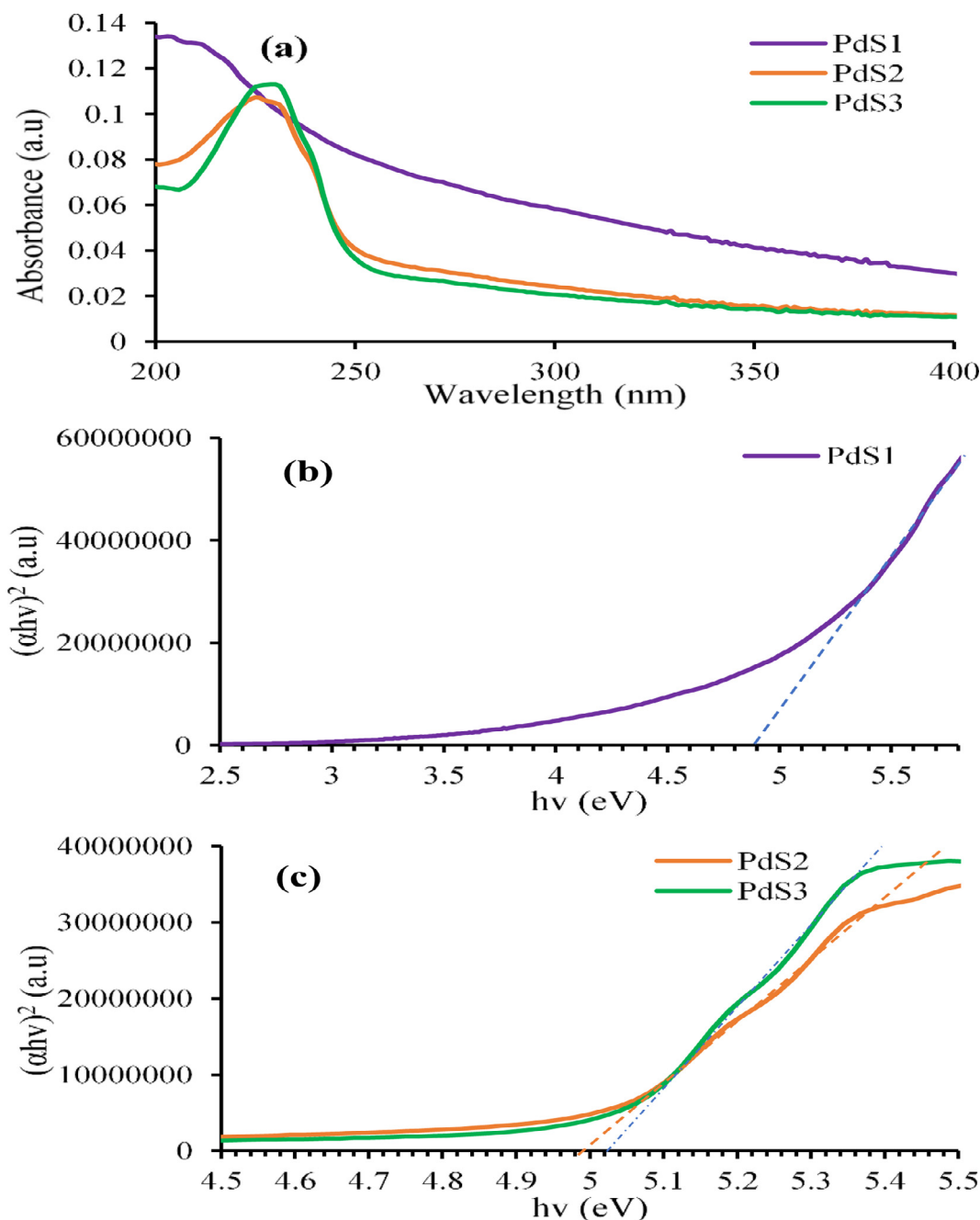


**Fig. 2.** Absorption spectra of PdS<sup>1</sup>, PdS<sup>2</sup> and PdS<sup>3</sup> (a), Tauc plot of PdS<sup>1</sup> (b) and PdS<sup>2</sup> and PdS<sup>3</sup> (c) and emission spectra of PdS<sup>1</sup>, PdS<sup>2</sup> and PdS<sup>3</sup> (d) nanoparticles.

observed shift confirmed the successful coordination of the two ligands to the metal ion.

### 3.3. Optical studies of PdS nanoparticles

The optical properties of the as-prepared PdS nanoparticles were studied by means of UV-Vis and photoluminescence spectroscopy. UV-Vis spectroscopy was used to observe the absorption of the PdS nanoparticles in DMSO, which correlates with the electron excitation from the valence band to conduction band [53]. The absorption spectra of the nanoparticles are illustrated in Fig. 2(a). PdS<sup>1</sup> showed no noticeable excitonic maximum. The spectra displayed band edges at 295, 258 and 264 nm for nanoparticles labelled PdS<sup>1</sup>, PdS<sup>2</sup> and PdS<sup>3</sup>, respectively. The optical absorption for

the PdS nanoparticles appeared at lower wavelength (blue-shifted) due to the quantum confinement influence of the nanoparticles particle size in comparison to bulk PdS [54]. Tauc plots were used to determine the optical band gap of the PdS nanoparticles where  $(\alpha h\nu)^2$  against  $h\nu$  was plotted. The optical band gap was obtained by extrapolating the linear region of the plot to  $(\alpha h\nu)^2 = 0$  as shown in Fig. 2(b,c). The optical band gaps were found to be 4.90, 4.98 and 5.02 eV for PdS<sup>1</sup>, PdS<sup>2</sup> and PdS<sup>3</sup>, respectively. Increase in temperature resulted in slight increase in the band gap values. The obtained optical band gap values were higher than the reported values found in literature [55]. The increased band gap suggested that the as-prepared PdS nanoparticles have small particle sizes, and more atoms occupied the surface of the particles. The emission spectra are shown in Fig. 2(d). Broad emission maxima were

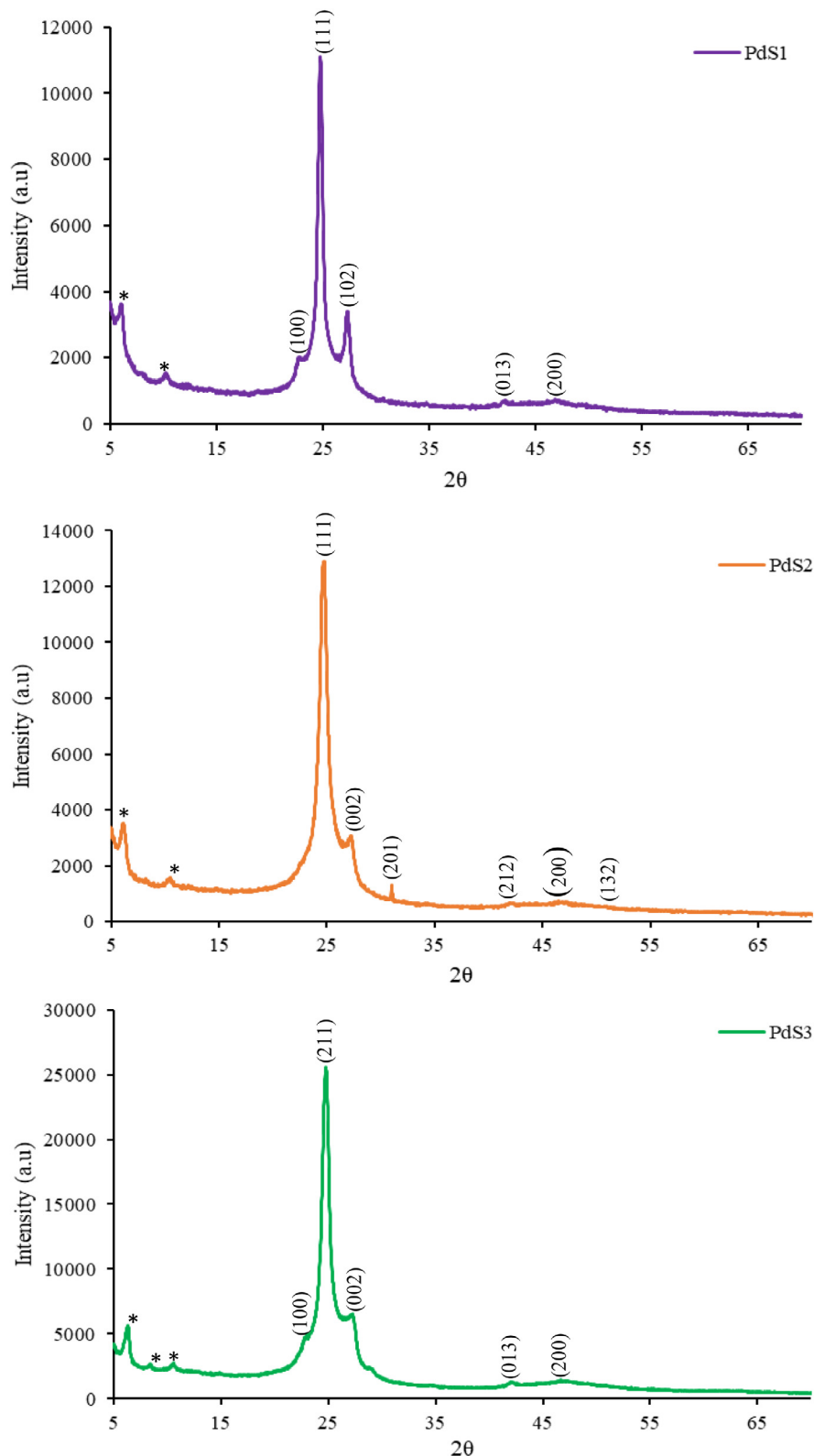


**Fig. 3.** pXRD spectra of PdS nanoparticles prepared at different temperatures.

observed at 389, 390 and 388 nm for PdS**1**, PdS**2** and PdS**3**, respectively. These are red shifted with respect to their absorption band edges. It was evident that variation of thermolysis temperature did not show any noticeable effect on the emission spectra of the PdS nanoparticles as the values obtained are almost equal.

### 3.4. Structural properties of PdS nanoparticles

#### 3.4.1. Powder X-ray diffraction (pXRD) of PdS nanoparticles

Palladium sulfide exist in several crystalline phases such as PdS,  $\text{Pd}_3\text{S}$ ,  $\text{Pd}_4\text{S}$ ,  $\text{Pd}_{16}\text{S}_7$  and  $\text{PdS}_2$  [28,56]. The pXRD patterns of the as-

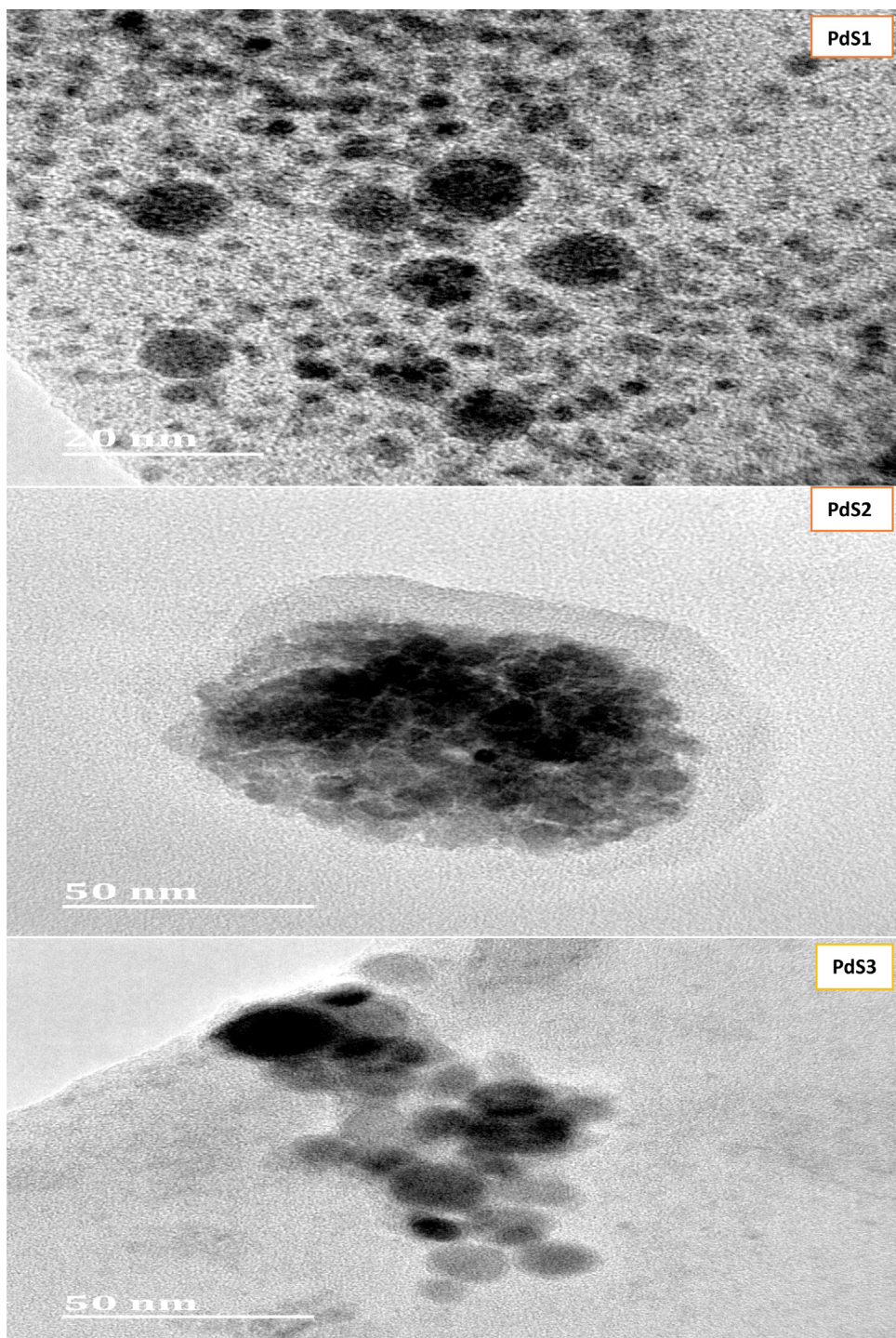


**Fig. 4.** HRTEM images of (a) PdS1, (b) PdS2 and (c) PdS3 nanoparticles.

prepared PdS nanoparticles shown in **Fig. 3** showed peaks at 22.94, 24.71, 42.60 and 47.00° which can be indexed to (100), (111), (102), (013) and (200) planes of a tetrahedral-Pd<sub>4</sub>S crystalline phase. PdS<sub>2</sub> nanoparticles showed diffraction patterns at 24.27, 27.27, 30.97, 41.86, 46.86 and 53.91° and can be indexed to (111), (002), (201), (212), (200) and (132) lattice planes of a tetragonal-PdS phase [57,58]. The diffraction patterns of PdS3 nanoparticles were observed at  $2\theta$  values of 23.18, 24.74, 42.67, 42.67 and 46.89° which correspond to (100), (211), (002), (013) and (200) lattice planes of a Pd<sub>4</sub>S crystalline phase [59]. The peaks denoted with (\*) are due to

the octadecylamine capping agent [60]. The obtained phases suggested that the decomposition temperature has an impact on the crystalline phases of the as prepared PdS nanoparticles.

#### 3.4.2. TEM images of the as-prepared PdS nanoparticles

HRTEM images of the nanoparticles are shown in **Fig. 4** and the TEM images are shown in Fig. S7. The PdS nanoparticles prepared at 160 °C is spherical in shape with particle size in the range 2.01–2.50 nm. The PdS nanoparticles prepared at 200 °C were clustered together and spherical in shape with particle sizes ranging be-

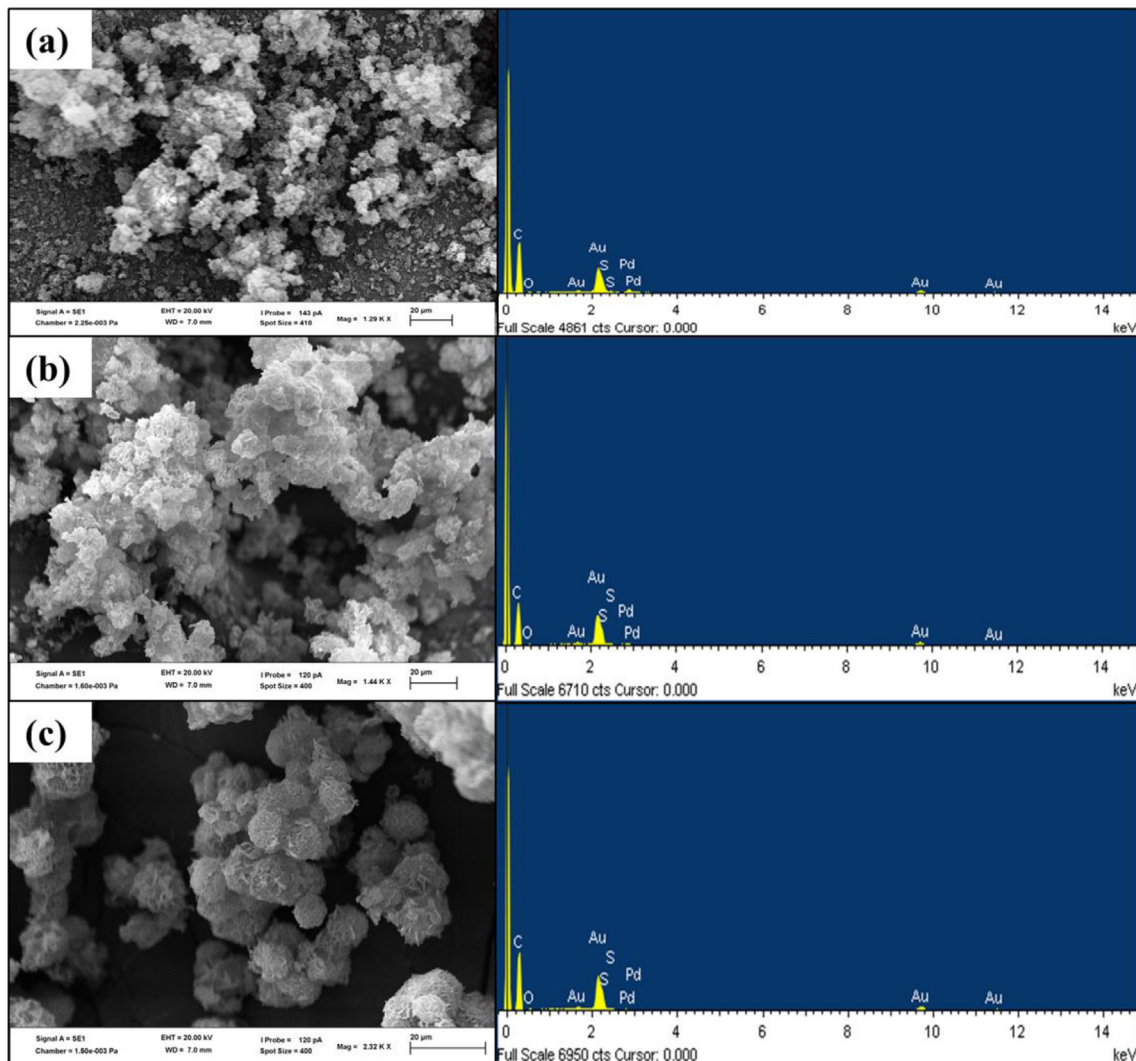


**Fig. 5.** SEM images and EDS spectra of (a) PdS1, (b) PdS2 and (c) PdS3.

tween 4.00 and 4.86 nm. The PdS prepared at 240 °C were unevenly distributed with particle sizes ranging between 2.53 and 4.12 nm. The results show that the nanoparticles increased in size when the temperature was raised from 160 to 200 °C, but at a higher temperature, uniform particles were obtained. When the temperature was raised to 240 °C, a mixture of small and large particles was obtained. It is evident that better nanoparticles are obtained at 200 °C.

SEM images and EDS spectra of PdS1, PdS2 and PdS3 nanoparticles are shown in **Fig. 5**. The nanoparticles were imaged at 20 μm. PdS1 nanoparticles prepared at 160 °C (**Fig. 5(a)**) showed flake-like surface morphology with no uniform pattern. PdS2 nanoparticles (**Fig. 5(b)**) also showed flake-like surface morphology but were more pronounced than PdS1 nanoparticles. PdS3 nanoparticles shown in **Fig. 5(c)** exhibited rough sweet thorn-like surface morphology. The smooth dark surfaces were due to the carbon tape used to fix the nanoparticles on the studs. The modifications noted on the surface morphologies of the as-prepared PdS nanoparticles implies that the decomposition temperature influence the formation of the nanoparticles resulting in the nanoparticles with different morphologies. The EDS spectra showed the Pd and S atoms, confirming the successful fabrication of the PdS nanoparticles. The C and O atoms were from the capping agent and

the double-sided carbon tape. And the Au atom was from the gold that was used to coat the nanoparticles for imaging [61].

### 3.5. FTIR studies of the PdS nanoparticles

FTIR spectra of octadecylamine (ODA) and the ODA capped PdS nanoparticles are shown in **Fig. 6**. The PdS nanoparticles spectra were compared with that of pure ODA spectrum. The spectra have few distinctions confirming the interaction of the PdS nanoparticles with the capping agent. Of note is the three absorption bands at 3326, 3248 and 3166 cm<sup>-1</sup> observed in the spectrum of ODA ascribed to ν(N-H) stretching vibrations [62,63]. These bands were not evident in the spectra of the PdS nanoparticles, suggesting that the capping of the nanoparticles occurred through the -NH<sub>2</sub> group of ODA capping agent. The variation of the stretching vibrations intensities from the PdS nanoparticles spectra signifies that nanoparticles prepared at different temperatures interact differently with the capping agent. The nanoparticles prepared at 160 and 200 °C exhibited low intensity and those at 240 °C showed high intensity. The high intensity observed in the PdS3 spectrum might be due to the random size distribution of the nanoparticles compared to that of PdS1 and PdS2 which showed uniform size distribution as shown in the TEM images (**Fig. 4**).

## 4. Conclusion

In this study, bis-(*N*-ethylphenyldithiocarbamato)palladium(II) was synthesized and characterized using elemental analysis, spectroscopic techniques and single crystal X-ray crystallography. The compound crystallized in a monoclinic space group  $P2_1/n$  in which the Pd(II) ion coordinate two molecules of *N*-ethylphenyldithiocarbamato anions to form a distorted square planar geometry. The complex was thermolyzed in octadecylamine (ODA) at 160, 200 and 240 °C to prepared ODA capped PdS nanoparticles and investigate the influence of thermolysis temperature on the morphological and optical properties of the PdS nanoparticles. Tetrahedral-Pd<sub>4</sub>S crystalline phases were obtained for nanoparticles prepared at 160 and 240 °C, whereas tetragonal-PdS phase was obtained for PdS nanoparticles prepared at 200 °C. PXRD patterns of the as-prepared nanoparticles proved that different crystalline phases were obtained by varying the temperature. The surface morphology of the as-prepared nanoparticles was investigated by TEM/HRTEM and SEM/ EDS. The TEM/HRTEM analysis revealed PdS1 nanoparticles are spherically shaped with some particles agglomerated to larger particles with particle sizes ranging between 2.01 and 2.50 nm. PdS2 nanoparticles were monodispersed spherically shaped with sizes of 4.00–4.86 nm. The PdS3 were randomly distributed with particle sizes of 2.53–4.12 nm. SEM micrographs of PdS1, PdS2 and PdS3 nanoparticles revealed that the thermolysis temperature plays a role on the surface morphology of the nanoparticles. Absorption and emission studies indicates that thermolysis temperature influence the energy band gap of the as-prepared PdS nanoparticles but does not have any significant effect on the emission properties of the PdS nanoparticles. A red shift was observed in the emission spectra in comparison to the absorption spectra. FTIR spectra study showed that PdS nanoparticles were stabilized with the ODA capping agent through the nitrogen atoms of the capping agent.

## Declaration of Competing Interest

The authors declare that they have no known competing financial interests or personal relationships that could have appeared to influence the work reported in this paper.

## CRediT authorship contribution statement

**Athandwe M. Paca:** Data curation, Formal analysis, Writing – original draft. **Peter A. Ajibade:** Conceptualization, Formal analysis, Funding acquisition, Project administration, Supervision, Writing – review & editing.

## Acknowledgments

The authors acknowledge the award of research grant by National Research Foundation, South Africa.

## Supplementary materials

Supplementary material associated with this article can be found, in the online version, at [doi:10.1016/j.molstruc.2021.130777](https://doi.org/10.1016/j.molstruc.2021.130777).

## References

- [1] A. Gaiardo, B. Fabbri, V. Guidi, P. Bellutti, A. Giberti, S. Gherardi, L. Vanzetti, C. Malagù, G. Zonta, Metal sulfides as sensing materials for chemoresistive gas sensors, *Sensors* 16 (2016) 1–19.
- [2] C. Rao, K. Pisharody, Transition metal sulfides, *Prog. Solid State Chem.* 10 (1976) 207–270.
- [3] S. Gross, A. Vittadini, N. Dengo, functionalisation of colloidal transition metal sulphides nanocrystals: a fascinating and challenging playground for the chemist, *Crystals* 7 (4) (2017) 110 <https://doi.org/10.3390/crys7040110>.
- [4] S. Rühle, M. Shalom, A. Zaban, Quantum-dot-sensitized solar cells, *Chem. Phys. Chem.* 11 (2010) 2290–2304.
- [5] C.-H. Lai, M.-Y. Lu, L.-J. Chen, Metal sulfide nanostructures: synthesis, properties and applications in energy conversion and storage, *J. Mater. Chem.* 22 (2012) 19–30.
- [6] Q.H. Wang, K. Kalantar-Zadeh, A. Kis, J.N. Coleman, M.S. Strano, Electronics and optoelectronics of two-dimensional transition metal dichalcogenides, *Nat. Nanotechnol.* 7 (2012) 699–712.
- [7] Y. Pan, Y. Liu, C. Liu, Phase-and morphology-controlled synthesis of cobalt sulfide nanocrystals and comparison of their catalytic activities for hydrogen evolution, *Appl. Surf. Sci.* 357 (2015) 1133–1140.
- [8] S. Mlowe, D.J. Lewis, M.A. Malik, J. Raftery, E.B. Mubofu, P. O'Brien, N. Revaprasadarao, Bis(piperidinedithiocarbamato)pyridinecadmium(II) as a single-source precursor for the synthesis of CdS nanoparticles and aerosol-assisted chemical vapour deposition (AACVD) of CdS thin films, *New J. Chem.* 38 (2014) 6073–6080.
- [9] N. Al-Dulaimi, D.J. Lewis, X.L. Zhong, M.A. Malik, P. O'Brien, Chemical vapour deposition of rhenium disulfide and rhenium-doped molybdenum disulfide thin films using single-source precursors, *J. Mater. Chem. C* 4 (2016) 2312–2318.
- [10] K. Krishnamoorthy, G.K. Veerasubramani, S.J. Kim, Hydrothermal synthesis, characterization and electrochemical properties of cobalt sulfide nanoparticles, *Mater. Sci. Semicond. Process.* 40 (2015) 781–786.
- [11] H. Emadi, M. Salavati-Niasari, A. Sobhani, Synthesis of some transition metal (M: <sup>25</sup>Mn, <sup>27</sup>Co, <sup>28</sup>Ni, <sup>29</sup>Cu, <sup>30</sup>Zn, <sup>47</sup>Ag, <sup>48</sup>Cd) sulfide nanostructures by hydrothermal method, *Adv. Colloid Interface Sci.* 246 (2017) 52–74.
- [12] K. Aiswarya, T. Raguram, K. Rajni, Synthesis and characterisation of nickel cobalt sulfide nanoparticles by the solvothermal method for dye-sensitized solar cell applications, *Polyhedron* 176 (2020) 114267.
- [13] X. Wang, S.-X. Zhao, L. Dong, Q.-L. Lu, J. Zhu, C.-W. Nan, One-step synthesis of surface-enriched nickel cobalt sulfide nanoparticles on graphene for high-performance supercapacitors, *Energy Storage. Mater.* 6 (2017) 180–187.
- [14] A.E. Oluwalana, P.A. Ajibade, Synthesis and crystal structures of Pb(II) dithiocarbamates complexes: precursors for PbS nanophotocatalyst, *J. Sulfur Chem.* 41 (2020) 182–199.
- [15] A.M. Paca, P.A. Ajibade, Effect of temperature on structural and optical properties of iron sulfide nanocrystals prepared from tris(*N*-methylbenzylidithiocarbamato)iron(III) complex, *Inorg. Nano-Met. Chem.* 51 (2021) 322–331.
- [16] N.H. Abdullah, Z. Zainal, S. Silong, M.I.M. Tahir, K.-B. Tan, S.-K. Chang, Synthesis of zinc sulphide nanoparticles from thermal decomposition of zinc *N*-ethyl-cyclohexyl dithiocarbamate complex, *Mater. Chem. Phys.* 173 (2016) 33–41.
- [17] C. Rao, S. Vivekchand, K. Biswas, A. Govindaraj, Synthesis of inorganic nanomaterials, *Dalton Trans.* (2007) 3728–3749.
- [18] N.L. Botha, P.A. Ajibade, Effect of temperature on crystallite sizes of copper sulfide nanocrystals prepared from copper(II) dithiocarbamate single source precursor, *Mater. Sci. Semicond. Process.* 43 (2016) 149–154.
- [19] P.A. Ajibade, J.Z. Mbese, B. Omondi, Group 12 dithiocarbamate complexes: synthesis, characterization and X-ray crystal structures of Zn(II) and Hg(II) complexes and their use as precursors for metal sulfide nanoparticles, *Inorg. Nano-Met. Chem.* 47 (2017) 202–212.
- [20] S. Campisi, M. Schiavoni, C.E. Chan-Thaw, A. Villa, Untangling the role of the capping agent in nanocatalysis: recent advances and perspectives, *Catalysts* 6 (2016) 1–21.
- [21] R.M. Crooks, M. Zhao, L. Sun, V. Chechik, L.K. Yeung, Dendrimer-encapsulated metal nanoparticles: synthesis, characterization, and applications to catalysis, *Acc. Chem. Res.* 34 (2001) 181–190.
- [22] P. Raveendran, J. Fu, S.L. Wallen, Completely “green” synthesis and stabilization of metal nanoparticles, *J. Am. Chem. Soc.* 125 (2003) 13940–13941.
- [23] D.J. Gavia, Y.S. Shon, Catalytic properties of unsupported palladium nanoparticle surfaces capped with small organic ligands, *Chem. Cat. Chem.* 7 (2015) 892–900.
- [24] D.K. Smith, B.A. Korgel, The importance of the CTAB surfactant on the colloidal seed-mediated synthesis of gold nanorods, *Langmuir* 24 (2008) 644–649.
- [25] N.L. Pickett, P. O'Brien, Syntheses of semiconductor nanoparticles using single-molecular precursors, *Chem. Rec.* 1 (2001) 467–479.
- [26] J.-H. Shim, B.-J. Lee, Y.W. Cho, Thermal stability of unsupported gold nanoparticle: a molecular dynamics study, *Surf. Sci.* 512 (2002) 262–268.
- [27] A. Roffey, N. Hollingsworth, G. Hogarth, Synthesis of ternary sulfide nanomaterials using dithiocarbamate complexes as single source precursors, *Nanoscale Adv.* 1 (2019) 3056–3066.
- [28] M.A. Ehsan, H.N. Ming, V. McKee, T.A.N. Peiris, U. Wijayantha-Kahagalage-Gamage, Z. Arifin, M. Mazhar, Vysotskite structured photoactive palladium sulphide thin films from dithiocarbamate derivatives, *New J. Chem.* 38 (2014) 4083–4091.
- [29] P. Ajibade, A. Nqombolo, Synthesis and structural studies of nickel sulphide and palladium sulphide nanocrystals, *Chalcogenide Lett.* 13 (2016) 427–434.
- [30] D.C. Onwudiwe, P.A. Ajibade, Synthesis and characterization of metal complexes of *N*-alkyl-*N*-phenyl dithiocarbamates, *Polyhedron* 29 (2010) 1431–1436.
- [31] G.M. Sheldrick, Crystal structure refinement with SHELXL, *Acta Crystallogr. C Struct. Chem.* 71 (2015) 3–8.
- [32] G.M. Sheldrick, SHELXT—Integrated space-group and crystal-structure determination, *Acta Crystallogr. A Found. Adv.* 71 (2015) 3–8.
- [33] W. Liu, H. Duan, D. Wei, B. Cui, X. Wang, Stability of diethyl dithiocarbamate chelates with Cu(II), Zn(II) and Mn(II), *J. Mol. Struct.* 1184 (2019) 375–381.
- [34] A.N. Gupta, V. Kumar, V. Singh, K.K. Manar, M.G. Drew, N. Singh, Intermolec-

- ular anagostic interactions in group 10 metal dithiocarbamates, *Cryst. Eng. Comm.* 16 (2014) 9299–9307.
- [35] G.I. Ndukwe, J.U. Nzeneri, O.J. Abayeh, Antibacterial assay of two synthesized dithiocarbamate ligands, *Am. J. Chem. Appl.* 5 (2018) 51–57.
- [36] R.P. Singh, V.K. Maurya, B. Maiti, K.A. Siddiqui, L.B. Prasad, Three new homoleptic nickel(II) 1, 1-dithiocarbamate complexes: synthesis, structure, electrical conductivity and DFT study, *J. Coord. Chem.* 71 (2018) 3008–3020.
- [37] R. Mohamad, N. Awang, N.F. Kamaludin, N.U. Pim, Spectral characterization and X-ray crystallographic studies of some triphenyltin(IV) dithiocarbamates compounds, *Asian J. Chem.* 30 (2018) 2743–2748.
- [38] S. Balakrishnan, S. Duraisamy, M. Kasi, S. Kandasamy, R. Sarkar, A. Kumarasamy, Syntheses, physicochemical characterization, antibacterial studies on potassium morpholine dithiocarbamate nickel(II), copper(II) metal, complexes and their ligands 5 (2019) 1–6 Heliyon.
- [39] M. Saeidifar, H. Mansouri-Torshizi, A.A. Saboury, Biophysical study on the interaction between two palladium(II) complexes and human serum albumin by Multispectroscopic methods, *J. Lumin.* 167 (2015) 391–398.
- [40] F. Hayat, R.F. Ali, Z. ur Rehman, F. Bélanger-Gariépy, Molecular, supramolecular, DNA-binding and biological studies of piperazine and piperidine based dithiocarbamates of biocompatible copper, *Inorg. Chem. Commun.* 121 (2020) 1–12.
- [41] H. Wang, J. Yang, P. Cao, N. Guo, Y. Li, Y. Zhao, S. Zhou, R. Ouyang, Y. Miao, Functionalization of bismuth sulfide nanomaterials for their application in cancer theranostics, *Chin. Chem. Lett.* 31 (2020) 3015–3026.
- [42] A. Birri, B. Harvey, G. Hogarth, E. Subasi, F. Uğur, Allyl palladium dithiocarbamates and related dithiolate complexes as precursors to palladium sulfides, *J. Organomet. Chem.* 692 (2007) 2448–2455.
- [43] S.Z. Khan, M.K. Amir, R. Abbasi, M.N. Tahir, Z. Rehman, New 3D and 2D supramolecular heteroleptic palladium(II) dithiocarbamates as potent anti-cancer agents, *J. Coord. Chem.* 69 (2016) 2999–3009.
- [44] D.V. Konarev, A.Y. Kovalevsky, A. Otsuka, G. Saito, R.N. Lyubovskaya, Neutral and ionic complexes of  $C_{60}$  with metal dibenzylidethiocarbamates. Reversible dimerization of  $C_{60}\bullet$ -in ionic multicomponent complex [Cr( $C_6H_5$ ) $_2\bullet$ ] $\cdot$ [ $C_{60}\bullet$ ] $\cdot$ 0.5[Pd(dbdtc) $_2$ ], *Inorg. Chem.* 44 (2005) 9547–9553.
- [45] F. Jian, F. Bei, P. Zhao, X. Wang, H. Fun, K. Chinnakali, Synthesis, crystal structure and stability studies of dithiocarbamate complexes of some transition elements ( $M=Co, Ni, Pd$ ), *J. Coord. Chem.* 55 (2002) 429–437.
- [46] H. Khan, A. Badshah, M. Said, G. Murtaza, J. Ahmad, B.J. Jean-Claude, M. Todorova, I.S. Butler, Anticancer metallopharmaceutical agents based on mixed-ligand palladium(II) complexes with dithiocarbamates and tertiary organophosphine ligands, *Appl. Organomet. Chem.* 27 (2013) 387–395.
- [47] J. Cheng, W. Wang, X. Xu, Z. Lin, C. Xie, Y. Zhang, T. Zhang, L. Li, Y. Lu, Q. Li, AgBi<sub>2</sub> nanoparticles with synergistic photodynamic and bioimaging properties for enhanced malignant tumor phototherapy, *Mater. Sci. Eng. C* 107 (2020) 1–9.
- [48] D.C. Onwudiwe, A.C. Ekenna, B.M.S. Mogwase, O.O. Olubiyi, E. Hosten, Palladium(II) and platinum(II) complexes of *N*-butyl-*N*-phenyldithiocarbamate: synthesis, characterization, biological activities and molecular docking studies, *Inorg. Chim. Acta* 450 (2016) 69–80.
- [49] V. Uivarosi, M. Badea, V. Aldea, L. Chirigu, R. Olar, Thermal and spectral studies of palladium(II) and platinum(IV) complexes with dithiocarbamate derivatives, *J. Therm. Anal. Calorim.* 111 (2013) 1177–1182.
- [50] L. Marcheselli, C. Preti, M. Tagliazucchi, V. Cherchi, L. Sindellari, A. Furlani, A. Papaioannou, V. Scarcia, Synthesis, characterization and evaluation of biological activity of palladium(II) and platinum(II) complexes with dithiocarbamic acids and their derivatives as ligands, *Eur. J. Med. Chem.* 28 (1993) 347–352.
- [51] T.J. Al-Hasani, M.K. Al-Taie, Synthesis, structural and antibacterial study of some metal ion dithiocarbamate-azo complexes, *Al-Nahrain J. Sci.* 18 (2015) 1–12.
- [52] J.Z. Mbese, P.A. Ajibade, Synthesis, structural and optical properties of ZnS, CdS and HgS nanoparticles from dithiocarbamate single molecules precursors, *J. Sulfur Chem.* 35 (2014) 438–449.
- [53] S. Afsheen, H. Naseer, T. Iqbal, M. Abrar, A. Bashir, M. Ijaz, Synthesis and characterization of metal sulphide nanoparticles to investigate the effect of nanoparticles on germination of soybean and wheat seeds, *Mater. Chem. Phys.* (2020) 123–216.
- [54] A. Parveen, S. Agrawal, A. Azam, Band gap tuning and fluorescence properties of lead sulfide Pb<sub>0.9</sub>A<sub>0.1</sub>S (A: Fe, Co, and Ni) nanoparticles by transition metal doping, *Opt. Mater.* 76 (2018) 21–27.
- [55] F. Samavat, F. Mahmoodi, P.T. Ahmad, M.F. Samavat, M.H. Tavakoli, S. Hadidchi, Effect of annealing temperature on the optical properties of palladium thin film, *J. Phys. Chem.* (2012) 103–106.
- [56] Y. Liu, A.J. McCue, J. Feng, S. Guan, D. Li, J.A. Anderson, Evolution of palladium sulfide phases during thermal treatments and consequences for acetylene hydrogenation, *J. Catal.* 364 (2018) 204–215.
- [57] M. Barawi, I. Ferrer, J. Ares, C. Sánchez, Hydrogen evolution using palladium sulfide (PdS) nanocorals as photoanodes in aqueous solution, *ACS Appl. Mater. Interfaces* 6 (2014) 20544–20549.
- [58] M.A. Ehsan, H.N. Ming, V. McKee, T.A.N. Peiris, U. Wijayantha-Kahagal-Gamage, Z. Arifin, M. Mazhar, Vysotskite structured photoactive palladium sulfide thin films from dithiocarbamate derivatives, *New J. Chem.* 38 (2014) 4083–4091.
- [59] P. O'Brien, J. Waters, Deposition of Ni and Pd sulfide thin films via aerosol-assisted CVD, *Chem. Vap. Depos.* 12 (2006) 620–626.
- [60] C. Wang, Z. Liu, S. Wang, Y. Zhang, Preparation and properties of octadecylamine modified graphene oxide/styrene-butadiene rubber composites through an improved melt compounding method, *J. Appl. Polym. Sci.* 133 (2016) 1–9.
- [61] S. Sharif, K.S. Ahmad, Synthesis of palladium diethyldithiocarbamate complexes as precursor for the deposition of un-doped and copper sulfide doped thin films by a facile physical vapour deposition technique, *Optik* 218 (2020) 1–19.
- [62] N.Ahmad Daud, B.W. Chieng, N.A. Ibrahim, Z.A. Talib, E.N. Muhamad, Z.Z. Abidin, Functionalizing graphene oxide with alkylamine by gamma-ray irradiation method, *Nanomaterials* 7 (2017) 1–15.
- [63] J. Benítez, M. San-Miguel, S. Domínguez-Meister, J. Heredia-Guerrero, M. Salmerón, Structure and chemical state of octadecylamine self-assembled monolayers on mica, *J. Phys. Chem. C* 115 (2011) 19716–19723.